

Beam Pattern Evolution of an Adaptive Transmit Beamspace Beamformer

S. S. Irfan Hussain¹ and M. Imran Shiekh¹

¹ Electrical Engineering Department, University of Engineering & Technology (UET), Lahore, Pakistan

Abstract

This paper presents evolution of beam pattern of an Adaptive transmit beamspace beamformer(ATBBF) at the base station of a 3rd generation code division multiple access (3G-CDMA) system for Multiple input single output (MISO) per user wireless channel, bridging the respective interest of antenna and signal processing groups. ATBBF establishes a set of orthogonal beams in space, each of which is weighted by an adaptive beamspace weight. The overall beam pattern is determined by the superposition of beamspace weighted orthogonal beams. The ATBBF algorithm perturbs beamspace weights at the base station to generate even and odd beamspace weights which are time multiplexed with the pilot signal. The mobile feedbacks a single bit to indicate which of the two beamspace weights delivered more power. This weight becomes the new beamspace weight. The beamspace weights and the beam pattern continue to be updated, finally converging to the optimum. Simulations in single, double and triple multipath wireless channels demonstrate the unique evolution of ATBBF's beam pattern in relation to the convergence of its beamspace weights. The dependence of magnitude and convergence time of a beamspace weight upon the multipath wireless channel is clarified to understand this evolution.

Key Words: Transmit beamforming, adaptive beamforming, beamspace beamforming, linear antenna array, beam pattern

1. Introduction

Multi-antenna downlink transmission for up to four antennas has been specified in the Long term evolution (LTE) of Third generation wideband code division multiple access (3G WCDMA) standards for targeting higher data rates [1]. Beamforming has been defined in LTE as one of the multi-antenna transmission schemes [1]. These schemes can be implemented as Multiple-input multiple-output (MIMO) or MISO systems. At high data rates MIMO can provide large capacity improvement. MISO system retains its importance as it limits the cost and size of the mobile terminal. Also as stated in [2], at fix data rates, extra bandwidth available with MIMO becomes unnecessary as the system tends to be operating in power limited mode rather than in band limited mode.

Various Adaptive transmit beamforming (ATBF) algorithms have been proposed for MISO Frequency division duplex (FDD) systems (where the forward

channel is unknown) to maximize received power [2]-[5]. This maximization is provided by beamforming gain through formation of a beam in the desired direction and fading diversity gain through feedback from the mobile [3]. In [5] all forward channel coefficients are fed back which makes it impractical for wireless systems due to constraints in feedback channel [3].

In slow fading channels the rest of the ATBF methods [2]-[4] give optimum performance, while in fast fading channels they are outperformed by diversity Space time codes (STC) [2] [3]&[6]. The reason is that for fast fading channels the channel changes at a rate difficult for ATBF algorithms to track and STC (which does not require tracking) gives better performance. In [7] & [8] a combination of STC and beamforming was proposed. Knowledge of mean values of the forward channel and estimate of the forward channel is required in [7] and [8] respectively, necessitating large feedbacks. In order to improve performance in fast fading channels an algorithm was

needed that could provide both spatial diversity and beamforming with efficient feedback.

An ATBBF combines beamforming and spatial diversity by forming a beam in the desired direction by superposition of weighted orthogonal beams in space [9] & [10]. Therefore in [11], an ATBBF algorithm for ATBF was devised where the orthogonal beams were adaptively weighed. The feedback was based on the approach of Gradient sign feedback algorithm (GSF) [3], which has the most efficient feedback consisting of only one bit. Hence this method was named Beamspace gradient sign feedback algorithm (BGSF). This paper demonstrates and explains the unique evolution of ATBBF's beam pattern in relation with its beamspace weights as BGSF updates them towards optimum values. Dependence of beamspace weight's convergence time and magnitude on the multipath wireless channel is comprehended to explain the progression of ATBBF's beam pattern. The paper has been organized as follows: In section 2, the beam pattern of ATBBF is derived. Section 3 shows how the BGSF algorithm adapts beamspace weights of ATBBF. The last section presents simulations and explains the relationships and dependences observed in them followed by conclusions.

2. Beam pattern of an adaptive transmit beamspace beamformer

ATBBF can consists of a maximum of N transmit beamformers on an N element linear array (as shown in Figure 1) to produce N orthogonal beams as shown for a receive beamspace beamformer in [9]. The array is a standard Uniform linear array (ULA) with inter element distance d equal to half of the carrier wavelength i.e. $d = \frac{\lambda}{2}$. This array is aligned with the z -axis and centered at the origin. Further it consists of $N = 4$ isotropic antenna elements. The position vector of the n^{th} antenna array element is $p_n = z_n a_z$ with $z_n = (n - \frac{N-1}{2})d$. Each of the N transmit beamformers forms one orthogonal beam. The orthogonal beam directed towards broadside ($\theta=90$) is called the center beam. Center beam is formed by a Transmit beamformer (TBF) that weighs each element of the above ULA with uniform weights ($w_n = 1/N$). This ULA has isotropic elements therefore its beam pattern is equivalent to its array factor. Neglecting mutual coupling, its beam pattern/array factor from [12] is:

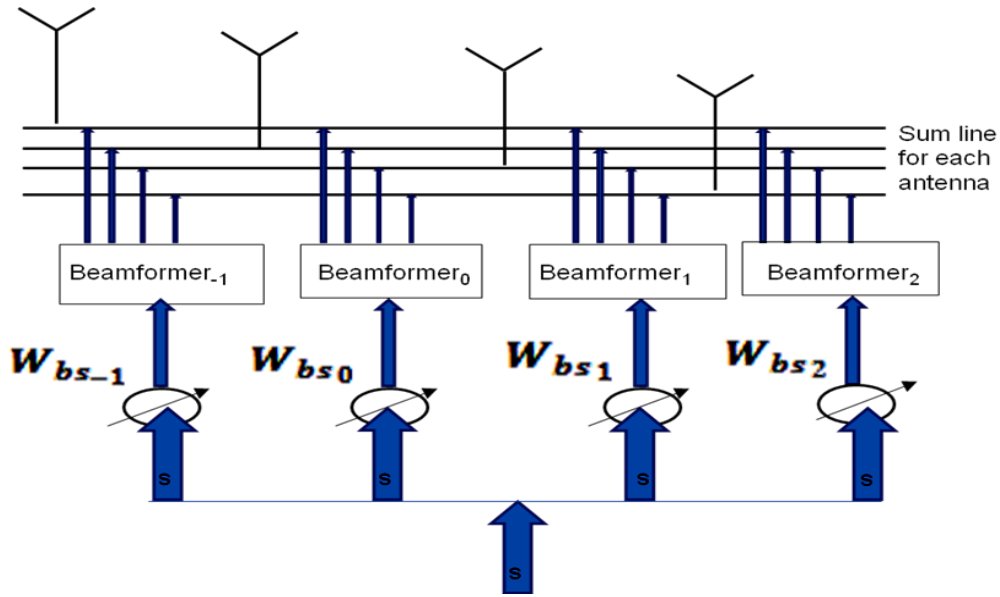


Figure 1: Schematic diagram of a ATBBF with $N = 4$ transmit beamformers

$$B(\theta) = \frac{1}{N} \frac{\sin\left(\frac{\pi N \cos \theta}{2}\right)}{\sin\left(\frac{\pi \cos \theta}{2}\right)} \quad (1)$$

Other orthogonal beams are formed on either side of the center beam by shifting it by specified values. This shift results in beams that are apart from each other by $2/N$ in spatial space ($\cos \theta$). Thus beams are mutually orthogonal as well as uniformly spread out in the total spatial span of 2 ($\cos \theta$ can vary from -1 to 1). The beam pattern of n^{th} TBF/orthogonal beam (from Eq. 1) for N even becomes:

$$B_n(\theta) = \frac{1}{N} \frac{\sin\left(\frac{\pi N}{2} \left(\cos \theta - \frac{2n}{N}\right)\right)}{\sin\left(\frac{\pi \cos \theta}{2}\right)}, n = -\frac{N}{2} + 1, \dots, \frac{N}{2} \quad (2)$$

E.g. for $N=4$, $n = -\frac{N}{2} + 1, \dots, \frac{N}{2} = -1, 0, 1, 2$. This gives the following values in spatial space where the orthogonal beams are shifted i.e. $\cos \theta = \frac{2}{N}(-1, 0, 1, 2) = \frac{-1}{2}, 0, \frac{1}{2}, 1$. In terms of elevation angle θ this amounts to $120^\circ, 90^\circ, 60^\circ, 0^\circ$ where the orthogonal beams are directed. The beam pattern of ATBBF is the sum of weighted beam patterns of the N transmit beamformers i.e.:

$$\begin{aligned} B_{ATBB}(\theta) &= \sum_{n=-\frac{N}{2}+1}^{\frac{N}{2}} W_{bs_n} B_n(\theta) \quad (3) \\ &= \sum_{n=-\frac{N}{2}+1}^{\frac{N}{2}} \frac{W_{bs_n}}{N} \frac{\sin\left(\frac{\pi N}{2} \left(\cos \theta - \frac{2n}{N}\right)\right)}{\sin\left(\frac{\pi \cos \theta}{2}\right)} \end{aligned}$$

Here W_{bs_n} is the n^{th} complex beamspace weight for weighing the n^{th} TBF beam pattern. For $N = 4$, beamspace weights $W_{bs_{-1}}, W_{bs_0}, W_{bs_1}, W_{bs_2}$ weigh beams directed at $120^\circ, 90^\circ, 60^\circ, 0^\circ$ respectively. Beam pattern of ATBB can also be expressed in terms of weights of the ULA elements for each TBF. Let $w(n)$ be the $N \times 1$ weight vector having weights of the n^{th} TB for all N elements of ULA. The weight vectors are also mutually orthogonal as their corresponding beam patterns are mutually orthogonal. Beam pattern of n^{th} TBF in terms of its weight vector is from [12]:

$$B_n(\theta) = v_k^H(k) w(n) \quad (4)$$

Here $k = \frac{2\pi}{\lambda} a_r$ denotes the wave number [9] of N plane waves from N respective antennas that become parallel at a far field point in direction of a_r . While the array manifold vector $v^k(k)$ defined in [9] and used in [12] evaluates for this ULA to:

$$v_k(k) = \begin{bmatrix} e^{-jk p_0} \\ e^{-jk p_1} \\ \vdots \\ e^{-jk p_{N-1}} \end{bmatrix} = \begin{bmatrix} e^{-j\pi(0-\frac{N-1}{2})\cos \theta} \\ e^{-j\pi(1-\frac{N-1}{2})\cos \theta} \\ \vdots \\ e^{-j\pi(N-1-\frac{N-1}{2})\cos \theta} \end{bmatrix} \quad (5)$$

ATBBF beam pattern becomes from Eq. 3 and Eq. 4:

$$B_{ATBB}(\theta) = \sum_{n=-\frac{N}{2}+1}^{\frac{N}{2}} v_k^H(k) w(n) W_{bs_n} \quad (6)$$

In order to accommodate all weight vectors in a matrix we define a $N \times N$ beamspace matrix B_{bs} , also known as the butler matrix. $w(n)$ weight vector is assigned to $(n + N/2)^{th}$ column of B_{bs} . Also we define $N \times 1$ beamspace weight vector w_{bs} having all the complex W_{bs_n} beamspace weights. Incorporating B_{bs} and w_{bs} in Eq. 6 we get:

$$B_{ATBB}(\theta) = v_k^H(k) B_{bs} w_{bs} \quad (7)$$

3. BGSF Algorithm

ATBBF as described above is at the base station of a 3G WCDMA system in a MISO wireless channel environment with single, double or triple multipath. Discrete time signal representation has been used by using the nyquist sampling theorem.

The signal to be sent to the mobile is s as shown in Figure 1. Assume that there are L multi paths. c_l is the $N \times 1$ channel vector representing all the complex channel coefficients of the l^{th} multipath. The n^{th} channel coefficient of c_l represents the path from the n^{th} antenna element to the mobile for l^{th} multipath.

Thus the received signal at the mobile (neglecting noise) from Eq. 7 and Figure 1 becomes:

$$r(m) = \sum_{i=1}^L c_l^H \frac{B_{bs} w_{bs}(i)}{\|B_{bs} w_{bs}(i)\|} s(m-l) \quad (8)$$

$$= \sum_{i=1}^L c_l^H \frac{B_{bs} w_{bs}(i)}{\|w_{bs}(i)\| / \sqrt{N}} s(m-l) \quad (9)$$

Multiple path terms in Eq. 9 have delays that are integral multiple of the Nyquist sampling time. Here i represents the i^{th} algorithm iteration of BGSF while m is the Nyquist sampling time index. The beamspace weights have been normalized so that concentration is on their direction rather than on their magnitude. Also, as columns of the beamspace matrix are orthogonal to one another i.e. $B_{bs}^H B_{bs} = \frac{1}{N}$ therefore denominator in Eq. 8 simplifies to

$$\|B_{bs} w_{bs}\| = \sqrt{(B_{bs} w_{bs})^H B_{bs} w_{bs}} = \frac{\|w_{bs}\|}{\sqrt{N}}$$

In this same i^{th} iteration, $w_{bs}(i)$, is also perturbed at the base station by a $N \times 1$ zero mean normal Gaussian vector p (having an autocorrelation matrix 21) to generate two pilot weights w_{bs_e} and w_{bs_o} as follows:

$$w_{bs_e}(i) = w_{bs}(i) + \|w_{bs}(i)\| \beta p(i) \quad (10)$$

$$w_{bs_o}(i) = w_{bs}(i) - \|w_{bs}(i)\| \beta p(i) \quad (11)$$

β is the adaptation rate parameter of the algorithm. There is provision of pilot signal s_p in the forward link of 3G CDMA systems for channel estimation at the mobile receiver used in coherent detection at the mobile [1]. A time slot of duration $Q=Mm$ (where M is any integer) is defined. A measurement interval equivalent to a specified integral multiple of $2Q$ is also defined. The pilot signal is sent with w_{bs_e} and w_{bs_o} in consecutive time slots i.e. with w_{bs_e} during even slots ($\lfloor \frac{m}{W} \rfloor = \text{even}$) and with w_{bs_o} during odd slots ($\lfloor \frac{m}{W} \rfloor = \text{odd}$). The received signal due

to the pilot signal in the even slot becomes (neglecting noise) from Eq. 9:

$$r_{pe}(m) = \sum_{i=1}^L c_l^H \frac{B_{bs} w_{bs_e}(i)}{\|w_{bs_e}(i)\| / \sqrt{N}} s(m-l) \quad (12)$$

While in the odd slot (neglecting noise) it is:

$$r_{po}(m) = \sum_{i=1}^L c_l^H \frac{B_{bs} w_{bs_o}(i)}{\|w_{bs_o}(i)\| / \sqrt{N}} s_p(m-l) \quad (13)$$

These pilot signals deliver even power $P_e^R(m)$ and odd power $P_o^R(m)$ in respective slots to the mobile. $P_e^R(m)$ is defined as square of $r_{pe}(m)$ divided by unit resistance [13] i.e. $P_e^R(m)$ is:

$$\left[\frac{\sum_{l=1}^L c_l^H B_{bs} w_{bs_e}(i) s_p(m-l)}{\|w_{bs_e}(i)\| / \sqrt{N}} \right] \times \left[\frac{\sum_{u=1}^L c_l^H B_{bs} w_{bs_e}(i) s_p(m-u)}{\|w_{bs_e}(i)\| / \sqrt{N}} \right] \quad (14)$$

Thus $P_e^R(m)$ is sum of L^2 product terms. Product terms having $l \neq u$ become zero. Hence Eq. 14 becomes

$$= \frac{\sum_{l=1}^L \|s_p(m-l)\|^2 [c_l^H B_{bs} w_{bs_e}(i)] [(B_{bs} w_{bs_e}(i))^H c_l]}{\|w_{bs_e}(i)\|^2 / N} \quad (15)$$

The power of the pilot sequence is one. There are scalar terms in each bracket. Scalar multiplication is commutative therefore reverse the order of the brackets to get:

$$P_e^R(m) = \frac{\sum_{l=1}^L w_{bs_e}^H(i) B_{bs}^H c_l c_l^H B_{bs} w_{bs_e}(i)}{\|w_{bs_e}(i)\|^2 / N} \quad (16)$$

Here $R = \sum_{l=1}^L c_l c_l^H$ can be substituted as the channel correlation matrix as defined in [3] & [6].

Similarly, $P_o^R(m)$ will have same expression consisting of w_{bs_o} instead of w_{bs_e} . Both above powers are summed separately for all even and odd slots in a particular measurement interval. The difference between summed even $\sum P_e^R(m)$ and odd $\sum P_o^R(m)$ power is found. The sign of this difference is fed back to the base station.

If the sign is positive the pilot signal sent with w_{bs_e} in even slots gave more power to the mobile while if the sign is negative pilot signal with w_{bs_o} gave more power in odd slots. Consequently, at the base station the beamspace weight w_{bs} for the next $(i+1)^{th}$ algorithmic iteration is w_{bs_e} for positive feedback, while it is w_{bs_o} for negative feedback.

The beamspace weights at the base station continue to be updated in this manner by BGSF, finally converging to those weights that result in forming a main lobe in the direction of the mobile.

4. Simulations and results

An ATBBF consisting of four TBF (as shown in Figure 1) on a four element ULA aligned along z-axis is simulated. BGSF algorithm is used to update ATBBF's beamspace weights. Initially the beamspace weights are taken as unity. The corresponding beam pattern (found by inserting these weights in Eq. 7) is the initial beam pattern (shown in Figure 2) for all simulations.

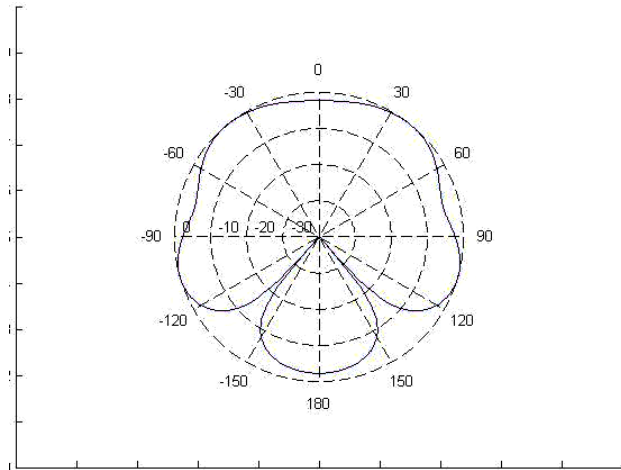


Figure 2: Initial beam pattern of ATBBF

Three wireless MISO channel scenarios have been separately simulated. The first, second and third channel scenarios consist of single, double and triple multipath having one, two and three channel vectors respectively. In a single multipath environment, signal energy arrives along a single path from an antenna to a mobile. While in double and triple multipath environments, signal energy from an antenna follows respectively two and three paths towards the mobile.

The gradual update of ATBBF's normalized beamspace weights by the BGSF algorithm and its corresponding normalized beam pattern have been depicted to show how this beam pattern gradually evolves into single / multiple lobes as the BGSF algorithm updates its beamspace weights. The relationship of beamspace weight's convergence time and its magnitude on various multipath wireless channels is illustrated to clarify this progression of ATBBF's beam pattern.

4.1 Simulation and results for a single multipath channels

In the first scenario the signal energy arrives at the mobile along a single path at $\theta = 105^\circ$ with respect to ULA at the base station (i.e. the channel vector is the array manifold vector in Eq. 5 with $\theta = 105^\circ$). Beam patterns of ATBBF for 10^{th} and 40^{th} iterations of BGSF are shown respectively in Figure 3 and Figure 4. Convergence of beamspace weights is shown in Figure 5. Beamspace weight $W_{bs_{-1}}$ and W_{bs_e} weights

the orthogonal beams directed at $\theta = 120^\circ$ and $\theta = 90^\circ$ respectively. The multipath signal direction $\theta = 105^\circ$ is in between the direction of these two beams. At the 10^{th} iteration both $W_{bs_{-1}}$ and W_{bs_e} converge and attain a magnitude of -2dB (Figure 5) resulting in the formation of a main lobe directed at $\theta = 105^\circ$ (Figure 3), while the other two weights have not yet converged (Figure 5). By the 40^{th} iteration the other weights i.e. W_{bs_1} and W_{bs_2} have already converged to a lower magnitude level of -6dB (Figure 5). This further enhances the directivity of the main lobe in the desired direction, but at the cost of an increased side lobe level (Figure 4). This shows that the convergence time and converged magnitude of a beamspace weight is dependent upon the proximity of its orthogonal beam to the multipath signal direction.

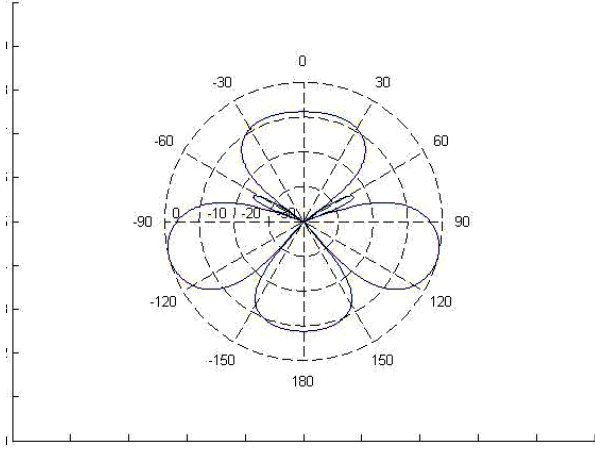


Figure 3: Beam pattern of ATBBF at 10th iteration of BGSF for multipath at $\theta = 105^\circ$

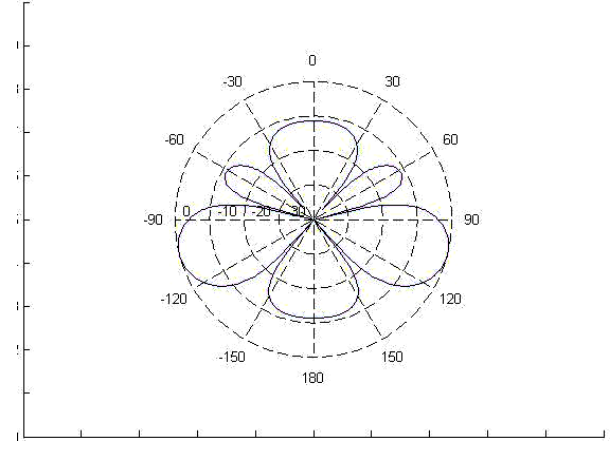


Figure 4: Beam pattern of ATBBF at 40th iteration of BGSF for multipath at $\theta = 105^\circ$

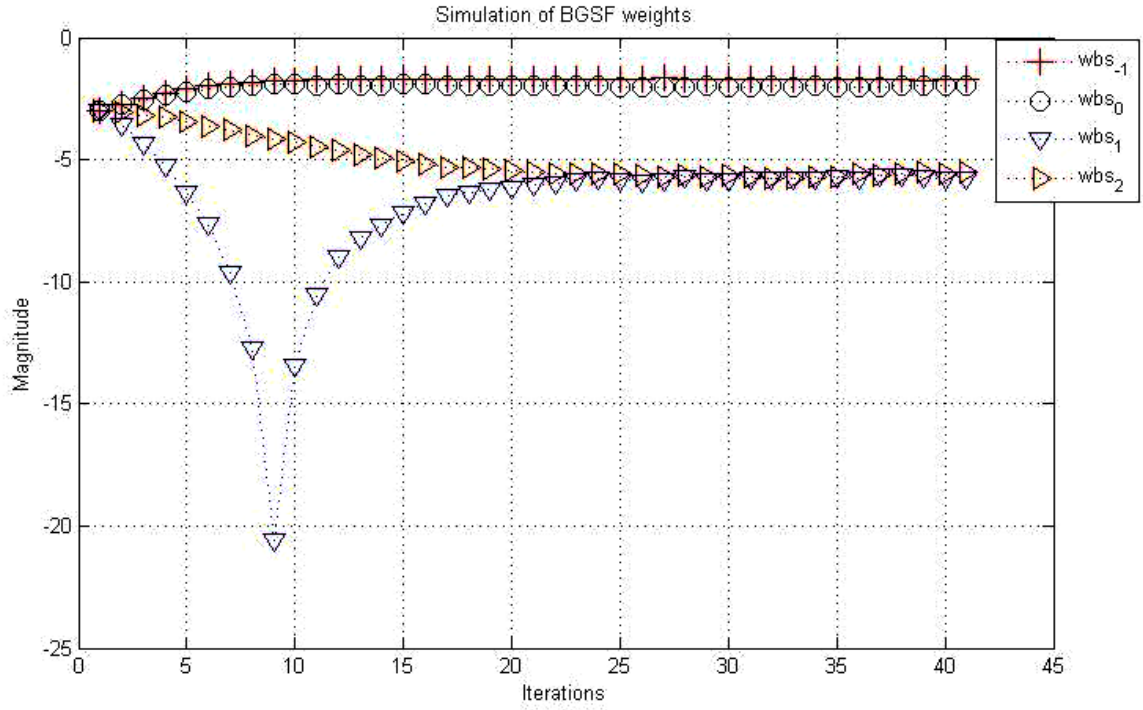


Figure 5: Convergence of beamspace weights of ATBBF for multipath at $\theta = 105^\circ$

Proximity is in terms of spatial space ($\cos\theta$) and not in terms angle of elevation (θ). This is verified by a second single multipath channel scenario with multipath signal direction at $\theta = 30^\circ$. This direction is equidistant to orthogonal beam directions of W_{bs_1} and W_{bs_2} in terms of θ . However W_{bs_2} acquires greater converged magnitude of 0db as compared to -5db of W_{bs_1} and converges earlier. The reason is that in spatial space this direction ($\cos 30=0.87$) is more towards orthogonal beam direction of W_{bs_2} ($\cos 0=1$). Thus closer the orthogonal beam is to a multipath signal direction in spatial space, greater is the magnitude of its beamspace weight on convergence and shorter is the time of convergence of its beamspace weight.

In order to verify the convergence of beamspace weights and beam pattern to optimal values, Eigen analysis was performed on the channel correlation matrix R for the first channel scenario. The principal eigenvector q was found to be:

$$q = [0.38 - 0.32i, -0.03 - 0.5i, \quad 0.34 - 0.36i,$$

q is the optimal weight vector of TB for R [3]&[6]. The optimal beam pattern can be found by substituting $w(n)=q$ in TBF's beam pattern expression i.e. Eq. 4. This beam pattern completely matches with the beam pattern of ATBB in the 40th iteration (Figure 4). Hence optimal beam pattern and beamspace weights of ATBB are achieved.

5. Simulation and results for double multipath

In this simulation, signal energy for the first multipath comes along $\theta = 0^\circ$, while for the second it comes along $\theta = 90^\circ$, with respect to the ULA at the base station. Beam pattern of ATBBF for 10th and 40th iterations of BGSF are given in Figure 6, and Figure 7 respectively. Convergence of beamspace weights is depicted in Figure 8. The two paths are at angles $\theta = 0^\circ$ and $\theta = 90^\circ$ where the orthogonal beams weighed by W_{bs_2} and W_{bs_e} are directed respectively.

At the 10th iteration both W_{bs_2} and W_{bs_e} converge and acquire -1.5dB magnitude (in Figure 8) resulting in the formation of lobes in the direction of $\theta = 0^\circ$ and $\theta = 96^\circ$ (in Figure 6). By the 40th iteration other weights i.e. $W_{bs_{-1}}$ and W_{bs_1} have already converged to lower magnitudes around -20dB (in Figure 8). This further enhances the directivity of lobes at $\theta = 0^\circ$ and $\theta = 96^\circ$ (in Figure 7).

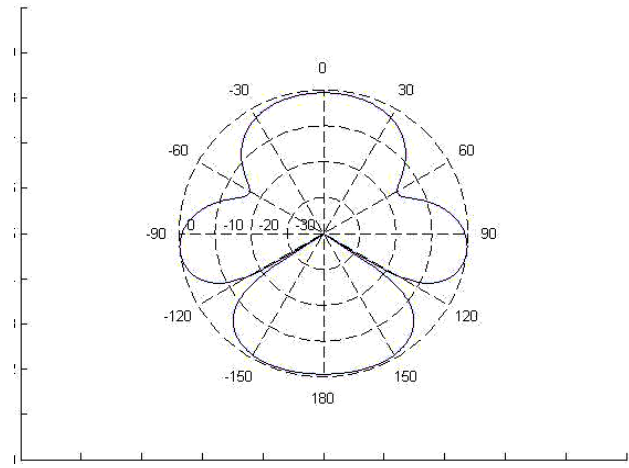


Figure 6: Beam pattern of ATBBF at 10th iteration of BGSF for first and second multipath at $\theta = 0^\circ$ and 90° respectively

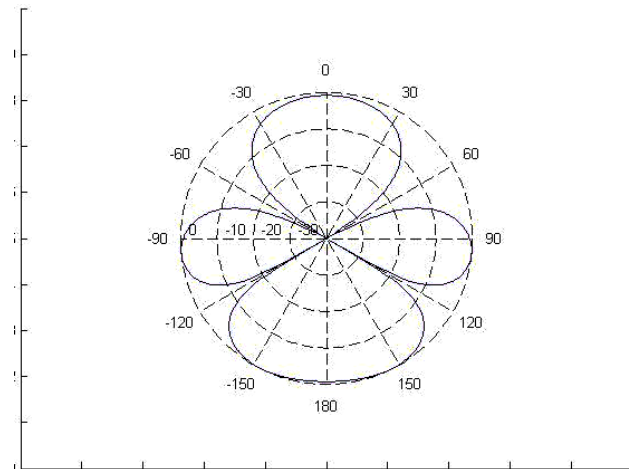


Figure 7: Beam pattern of ATBBF at 40th iteration of BGSF for first and second multipath at $\theta = 0^\circ$ and 90° respectively

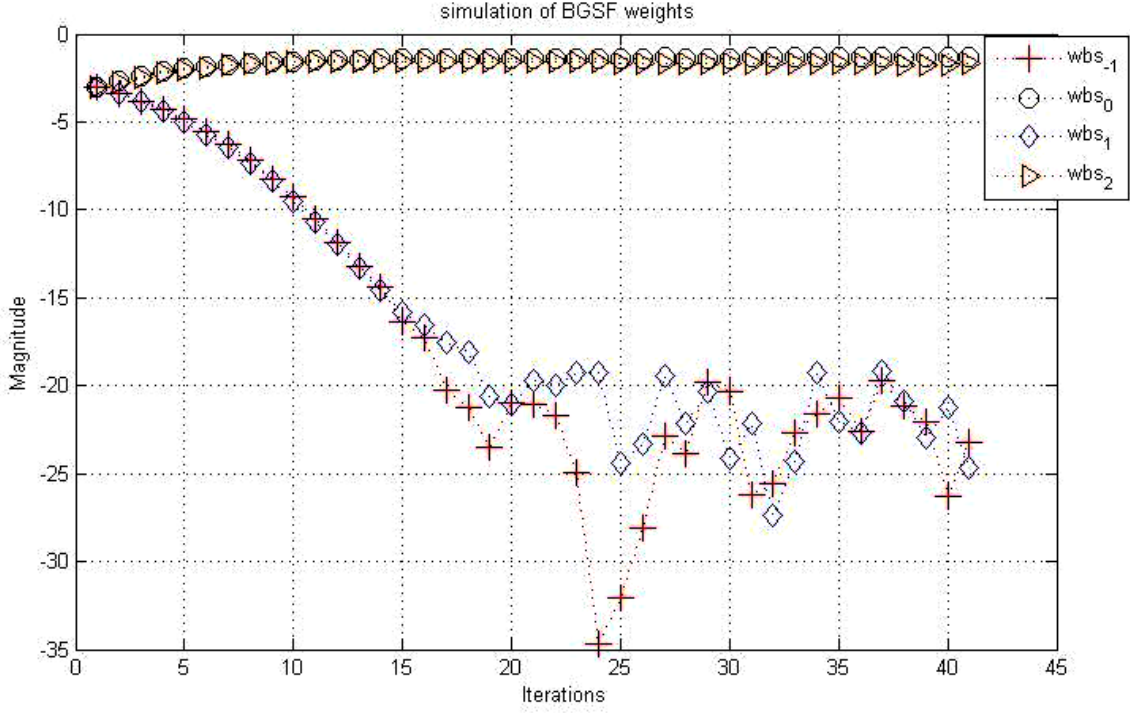


Figure 8: Convergence of beamspace weights of ATBBF for first and second multipath at $\theta = 0^\circ$ and 90° respectively

Finally, as the required directions were along orthogonal beams, lobes were not achievable simultaneously in both directions. This results in a slight shift in the direction of one of the two lobes.

In order to confirm convergence to optimal beamspace weights and beam pattern the two principal eigenvectors of the channel correlation matrix R for this channel scenario were found. One of them is:

$$q = [-0.58i, 0.41, -0.58i, 0.41]^T$$

The optimal beam pattern (corresponding to $w(n)=q$ in Eq. 4) completely matches with the final beam pattern of BGSF in the 40th iteration (Figure 7). Hence optimal beam pattern and beamspace weights are achieved.

This double path simulation confirms the findings from single multipath case. There are also some subtle observations not seen in single multipath case. Table 1 depicts observations for several double

Table 1: Double multipath channel simulations

Multipath signal direction θ (in degrees)		Convergence time of beamspace weights (No of iterations)				Normalized magnitude of converged beamspace weight (dB)			
First	Second	W_{bs-1}	W_{bs0}	W_{bs1}	W_{bs2}	W_{bs-1}	W_{bs0}	W_{bs1}	W_{bs2}
0°	105°	13	9	12	7	-4	-4	-8	-1
0°	108°	9	12	14	7	-3	-5	-8	-1
0°	112°	3	14	12	8	-2	-7	-9 to -10	-1
0°	116°	3	14	15	11	-2	-10	-11to-12	-1
0°	120°	3	13	12	3	-1or-2	<-16	<-15	-2

multipath simulations. Here the first multipath signal direction remains along $\theta = 0^\circ$ while the second is gradually shifted from $\theta = 105^\circ$ to $\theta = 120^\circ$.

The third and fourth row of Table 1 shows that the convergence time of $W_{bs_{-1}}$ becomes less than that of W_{bs_2} . This is despite the fact that there is a multipath direction along orthogonal beam of W_{bs_2} while there is none along orthogonal beam of $W_{bs_{-1}}$. The reason is that firstly the second multipath direction is close to the orthogonal beam of $W_{bs_{-1}}$. This gives $W_{bs_{-1}}$ a short convergence time. Secondly second multipath is also not along orthogonal beam of $W_{bs_{-1}}$. This results in giving $W_{bs_{-1}}$ a converged magnitude (-2dB) closer to the initial value (-3dB) and lesser in comparison with that of W_{bs_2} (-1dB). These reasons cause $W_{bs_{-1}}$ to have shortest convergence time. The earlier convergence of $W_{bs_{-1}}$ results in forming a lobe towards the second multipath signal direction in advance to the formation of lobe towards the orthogonal beam direction of W_{bs_2} .

5.1 Simulation and results for triple multipath

In this triple multipath simulation, signal energy for the first, second and third multipath arrives along $\theta = 45^\circ, 90^\circ$ & 120° respectively, with respect to the ULA at the base station. Beam pattern of ATBBF for 10th and 40th iterations of BGSF algorithm are in Figure 9 and Figure 10. Convergence of beamspace weights is shown in Figure 11. The first multipath is at $\theta = 45^\circ$. This path is between orthogonal beams at $\theta = 60^\circ$ and $\theta = 0^\circ$ weighed by W_{bs_1} and W_{bs_2} respectively. W_{bs_1} converges earlier with higher magnitude around -3.5dB (in Figure 11) while W_{bs_2} converges latter with a lower magnitude of -5dB (in Figure 11) because the $\theta = 45^\circ$ multipath is closer to the $\theta = 60^\circ$ beam weighed by W_{bs_1} in spatial space. By the 10th iteration both these beamspace weight have converged. This results in the formation of a lobe towards $\theta = 45^\circ$ at the 10th iteration (in Fig 9).The

other two paths are at angles $\theta = 90^\circ$ and $\theta = 120^\circ$ in the direction of the orthogonal beams weighed by W_{bs_e} and $W_{bs_{-1}}$ respectively. Both these weights do not converge by the 10th iteration. Earlier convergence of W_{bs_1} is because the multipath signal direction of $\theta = 45^\circ$ is close to and not along the orthogonal beam direction of W_{bs_1} . Thus W_{bs_1} has short convergence time and its magnitude at convergence (-3.5dB) is closest to its initial magnitude (-3dB). This gives W_{bs_1} the fastest convergence.

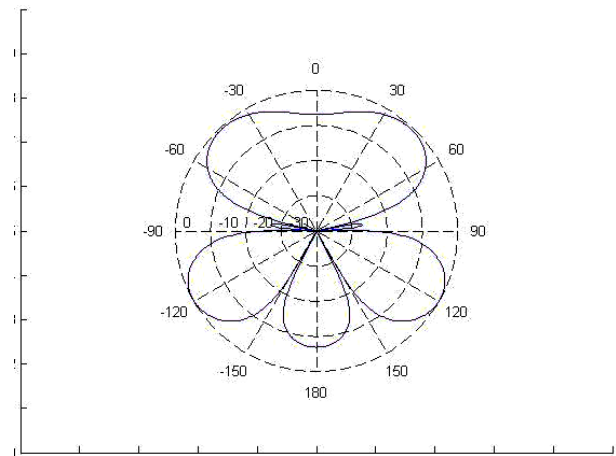


Figure 9: Beam pattern of ATBBF at 10th iteration of BGSF for first, second and third multipath at $\theta = 45^\circ, 90^\circ$ and 120° respectively

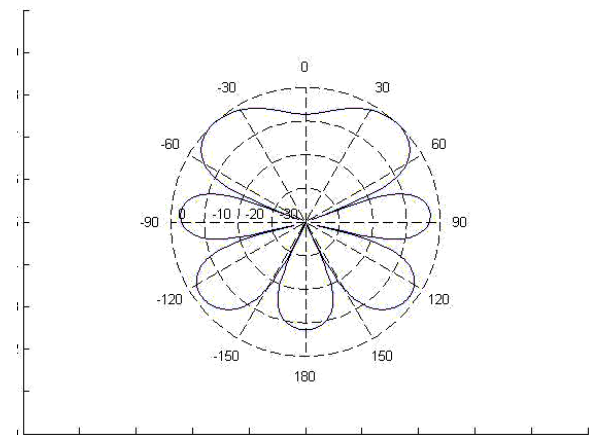


Figure 10: Beam pattern of ATBBF at 40th iteration of BGSF for first, second and third multipath at $\theta = 45^\circ, 90^\circ$ and 120° respectively.

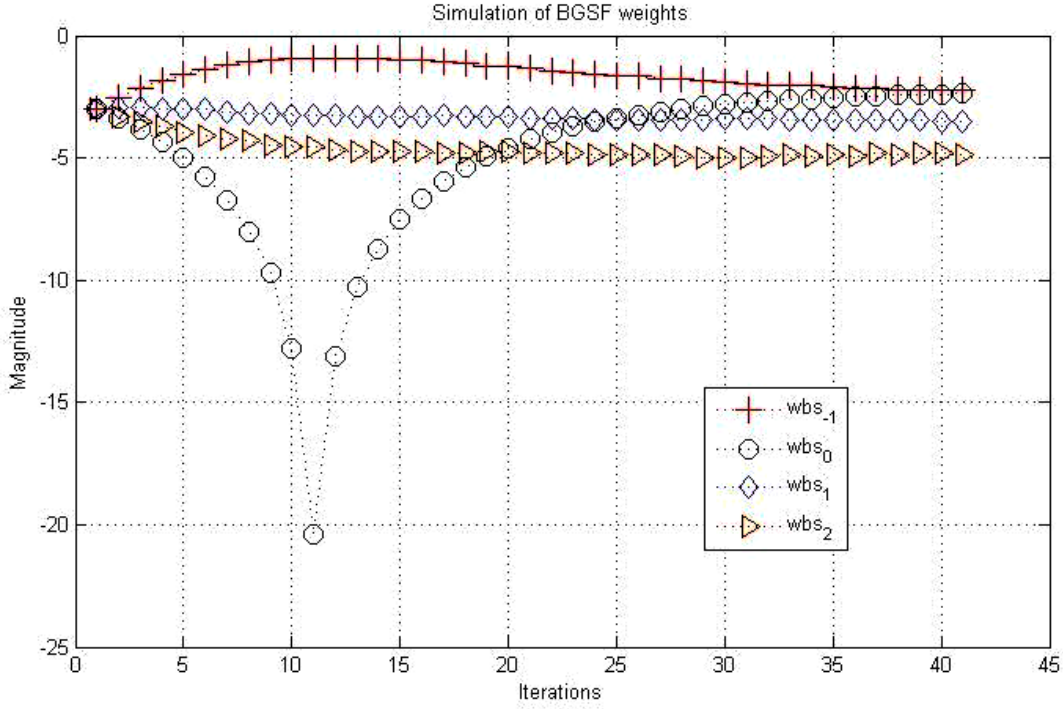


Figure 11: Convergence of beamspace weights of ATBBF for first, second and third multipath at $\theta = 45^\circ, 90^\circ$ and 120° respectively

By the 40th iteration both W_{bs_e} and $W_{bs_{-1}}$ converge to around -2.25 dB of magnitude (in Figure 11) which is greater than the magnitude of the other two weights W_{bs_1} and W_{bs_2} . This happens because there are multipath along the direction of beams weighed by W_{bs_e} and $W_{bs_{-1}}$ while no multipath exists along beams weighed by W_{bs_1} and W_{bs_2} . Convergence of beamspace weight W_{bs_e} and $W_{bs_{-1}}$ by the 40th iteration results in the formation of lobes directed at $\theta = 87^\circ$ and $\theta = 126^\circ$ (in Figure 10). There is a slight shift in the directions of these two lobes from their desired directions as lobes cannot be formed at the same time in both orthogonal directions.

Eigen analysis of the channel correlation matrix R for this channel scenario reveals that there is one principal eigenvector q as given below:

$$q = [-0.57 + 0.39i, -0.02 - 0.14i, -0.1 + 0.1i, 0.69]^T$$

The optimal beam pattern (corresponding to $w(n)=q$ in Eq. 4) completely matches with the final beam pattern of BGSF in the 40th iteration (in Figure 10). Hence optimal beam pattern and beamspace weights are achieved.

6. Conclusions

Evolution of beam pattern of ATBBF has been presented. ATBBF generates a set of orthogonal beams equal to or less than the number of antenna elements. A specific weight vector corresponds to an orthogonal beam. Therefore a set of such weight vectors can be applied to form orthogonal beams. In addition, a "beamspace weight" weighs an orthogonal beam's weight vector. The BGSF algorithm updates beamspace weights of the ATBBF in such a way that as the beamspace weights converge, the corresponding beam pattern gradually produces and directs multiple lobes. These multiple lobes correspond to directions of multipath signals towards the mobile. Simulations are produced for single, double and triple multipath scenarios.

The single multipath channel simulation shows that the beamspace weights of the respective orthogonal beams closer (in terms of spatial space) to the multipath signal direction converge earlier to a greater magnitude. This results in ATBBF forming a main lobe exactly towards required direction. Other beamspace weights converge later, ensuing increased directivity of the main lobe. This shows that on applying BGSF, ATBBF forms a main lobe in the desired direction before complete convergence is achieved.

The double multipath channel simulation illustrates that lobes are formed towards the two multipath signal directions. Lobe for multipath signal direction along an orthogonal beam is formed earlier while lobe for other multipath signal direction is formed afterwards in accordance with single multipath channel observations. However lobe for multipath signal direction not along an orthogonal beam can form earlier provided this direction is close to an orthogonal beam's direction. This gives the beamspace weight of that orthogonal beam a short convergence time and a converged magnitude close to its initial value. This leads to its earliest convergence forming a lobe in advance.

In the triple multipath simulation three lobes are formed. Lobe for multipath signal direction not along an orthogonal beam forms first. This is in accordance with the double multipath channel observation of multipath signal direction being close to an orthogonal beam direction. While lobes for multipath signal directions along orthogonal directions are formed later. Acquired magnitudes of converged beamspace weights for double and triple multipath channels follow the single multipath observation. The direction of a lobe in the double and triple multipath simulations has little or no offset from the desired direction.

This demonstrates that ATBBF with BGSF algorithm fairly utilizes the multipath directions present in MISO downlink channels by directing lobes towards them. Furthermore, the beam pattern and beamspace weights of an ATBBF with BGSF algorithm has been shown to converge to optimal beam pattern and beamspace weights for different channel scenarios. Lastly the observed relationships give ATBBF with BGSF algorithm an inherent potential to determine the downlink channel at the transmitter.

7. Acknowledgement

This research has been funded by the University of Engineering and technology (UET), Lahore and Higher education commission (HEC) of Pakistan.

8. References

- [1] K. Fazel and S. Kaiser; (2008). *Multi-carrier and spread spectrum systems*, John Wiley & Sons Ltd.
- [2] B. C. Banister and J. R. Zeidler; (2005). *IEEE Transactions on Wireless Communications*, vol. 4, no.3, 1121-1135
- [3] B. C. Banister and J. R. Zeidler; (2003). *IEEE Transactions on Signal Processing*, vol. 51, no.5, 1156-1171
- [4] R.W. Heath Jr and A. Paulraj; (1998). *In Conf. Rec. 32nd Asilomar conference on Signals, Systems and Computers*, vol. 2, 1073-1078.
- [5] D. Gerlach and A. Paulraj; (1994). *IEEE Signal Processing Letters*, vol. 1, no. 10, 150-152.
- [6] R. T. Derryberry, S. D. Gray, D. M. Ionescu, G. Mandyam and B. Raghothaman; (2002). *IEEE Communications Magazine*, vol. 40, issue. 4, 68-75.
- [7] S. Zhou and G. B. Giannakis; (2002). *IEEE Transactions on Signal Processing*, vol. 50, no.10, 2599-2614.
- [8] G. Jongren, M. Skoglund and B. Ottersten; (2002). *IEEE Transactions on Information theory*, vol. 48, no.3, 611-627
- [9] H. L. Van. Trees; (2002). *Optimum array processing*, John Wiley & Sons, Inc., New York.
- [10] J. Litva and T. K. Lo; (1996). *Digital beamforming in wireless communications*, Artech house Inc., Norwood, MA/
- [11] S. S. I. Hussain, M. I. Shiekh; (2007). *IEEE International Conference on Electrical Engineering*, Lahore, 1-6.
- [12] C. A. Balanis; (2005). *Antenna theory, analysis and design*, John Wiley & Sons, Inc., New Jersey.
- [13] B. Sklar; (2006). *Digital communications, Fundamentals and Applications*, Prentice hall, Upper saddle River, New Jersey.